Wang *et al. Microstructures* 2024;4:2024006
DOI: 10.20517/microstructures.2023.47

Microstructures

Research Article

Open Access

Check for updates

New vision of convection induced freckle formation theory in nickel-based superalloys by electron microscopy

Shuai Wang[1,#], Yuliang Jia[2,#], Yongzhe Wang[3,#], Yongjia Zhang[4], Lan Ma[5], Feng Cheng[1], Yi Zeng[3], Xu Shen[4], Yingliu Du[2], Binghui Ge[1]

[1]Information Materials and Intelligent Sensing Laboratory of Anhui Province, Institutes of Physical Science and Information Technology, Anhui University, Hefei 230601, Anhui, China.
[2]Anhui Yingliu Hangyuan Power Technology Co., Ltd, Huoshan 237200, Anhui, China.
[3]The State Key Lab of High Performance Ceramics and Superfine Microstructure, Shanghai Institute of Ceramics, Chinese Academy of Sciences, Shanghai 200050, China.
[4]State Key Laboratory of Materials Processing and Die & Mould Technology, School of Materials Science and Engineering, Huazhong University of Science and Technology, Wuhan 430074, Hubei, China.
[5]Department of Nano-analysis, The Oxford Instruments Technology China, Shanghai 200233, China.
[#]Authors contributed equally.

Correspondence to: Prof. Binghui Ge, Information Materials and Intelligent Sensing Laboratory of Anhui Province, Institutes of Physical Science and Information Technology, Anhui University, Hefei 230601, Anhui, China. E-mail: bhge@ahu.edu.cn; Prof. Yi Zeng, The State Key Lab of High Performance Ceramics and Superfine Microstructure, Shanghai Institute of Ceramics, Chinese Academy of Sciences, 1295 Dingxu Road, Shanghai 200050, China. E-mail: zengyi@mail.sic.ac.cn

How to cite this article: Wang S, Jia Y, Wang Y, Zhang Y, Ma L, Cheng F, Zeng Y, Shen X, Du Y, Ge B. New vision of convection induced freckle formation theory in nickel-based superalloys by electron microscopy. *Microstructures* 2024;4:2024006. https://dx.doi.org/10.20517/microstructures.2023.47

Received: 6 Sep 2023 **First Decision:** 20 Oct 2023 **Revised:** 29 Nov 2023 **Accepted:** 6 Dec 2023 **Published:** 12 Jan 2024

Academic Editors: Shujun Zhang, Xiaozhou Liao **Copy Editor:** Fangyuan Liu **Production Editor:** Fangyuan Liu

Abstract

Freckles, one of the common defects in blades used in heavy-duty gas turbines, hugely deteriorate the mechanical properties and liability of blades under service conditions. The thermal-solutal convection theory is a widely adopted formation mechanism, but few solid experimental pieces of evidence have been reported. Here, the grain microstructure in freckle chains taken from four different Nickel-based superalloys with either single-crystal or directionally solidified alloy is analyzed for the first time. The relationship between the internal stress and the misorientation throughout the freckle chains is studied by means of state-of-the-art electron microscopy. The results supply new experimental evidence of the thermal-solutal convection theory, which is further supported by the fact that borides at the boundary are randomly orientated to alloys. Therefore, this research enriches the methodology of freckle study, providing new insight into the formation mechanism of casting defects.

Keywords: Nickel-based superalloy, freckle, dendrite fracture, orientation, strain

© The Author(s) 2024. **Open Access** This article is licensed under a Creative Commons Attribution 4.0 International License (https://creativecommons.org/licenses/by/4.0/), which permits unrestricted use, sharing, adaptation, distribution and reproduction in any medium or format, for any purpose, even commercially, as long as you give appropriate credit to the original author(s) and the source, provide a link to the Creative Commons license, and indicate if changes were made.

INTRODUCTION

Operating under high temperatures and complex stress-corrosive environments, turbine blades put forward stringent requirements on relevant materials. Nickel-based superalloys are ideal for these applications thanks to their extraordinary properties, such as high-temperature strength, creep, and fatigue characteristics[1-3]. However, a series of casting defects formed during the directional solidification seriously affect the service performance[4,5]. For example, freckles are one of the common casting defects in heavy-duty gas turbine (HDGT) blades, wherein equiaxed crystal chains with a random orientation grow on the blade surface along the solidification direction, which introduces transverse grain boundaries into alloys[6,7].

In that regard, the possibility to predict or decrease the formation of freckles attracts a great deal of interest from researchers. Theoretically, the Rayleigh number as the ratio of the driving force to the resistance in solute convection is considered crucial in the prediction of the freckle formation[8]. However, for different alloy systems, the Rayleigh number should be corrected according to solidification conditions as an important reference[9-11]. Various experimental attempts have been made so far to avoid freckles, such as inversion solidification, mold tilting, and addition of a magnetic field[12-14]. Nevertheless, to improve the thermal efficiency of the gas turbine, the size of the turbine blade must be increased, and the aero-engine requires a more complex structural design[15]. On the other hand, the content of refractory elements, such as W and Re, has risen in recent years to improve the endurance temperature of the blade[2,7,16]. Both factors are found to enhance the tendency of freckle formation. Therefore, a deep understanding of the formation mechanism of freckles is of great significance for practical applications.

The thermal-solutal convection theory is widely accepted to explain the formation of freckles[2]. This is because solute segregation causes density inversion and solute convection in the channel, leading to the remelt or even fracture of dendrites, which eventually accounts for the presence of freckles[17]. Therefore, the formation of freckles requires two prerequisites: an open solute channel and sufficient thermal-solutal convection. It is reported that the overgrowth, deflection, and remelting of dendrites result in open solute channels whose survival depends on the competition among solute transport, lateral heat flux, and growth of dendrites[18-20]. On the other hand, considering that density inversion is the basis of solute convection, the partition coefficient as the mass fraction ratio of the elements between dendrite and inter-dendrite is an important parameter to evaluate the effect of different elements on freckle initiation[7,21]. Moreover, it has been found experimentally that the addition of C, W, Re, and Hf elements notably affects the extent of solute segregation and changes the convection intensity, thus regulating the formation of freckles[16,22-24].

In essence, freckles are believed to be the result of the fracture rotation of secondary dendrites. The secondary dendrites forming during the directional solidification enter the shear deformation under the coupling effect from both the remelt and solute convection[25,26]. As for the remelting, a solute (such as Al and Ti) enriched at the root of a secondary dendrite during solidification changes the local composition balance of a solid-liquid interface, making the root remelt[27-29]. In turn, for the stress induced by convection, it seems easier to understand that the thermal-solutal convection in supercooled melts exposes the secondary dendrites to shear deformation, causing the dendrites to bend[30-33]. Remelting enables easy achievement of the critical load value, allowing secondary dendrites to fracture and form freckles[34,35]. Concerning the above-mentioned solute-convection theory, some experimental[19,27,36] and computational studies[20,26,28,29,34] obtained on the macroscopic or mesoscopic scale have been reported to date. Nevertheless, the formation of freckles is a complex process[9], and there is still a lack of sufficient knowledge about the relevant mechanisms from the viewpoint of microstructures.

Electron microscopy is an important method to characterize the microstructure of materials. It can reveal not only the composition and element content but also the local crystal structure, including the orientation and strain distribution. Then, the formation mechanism of freckles can be deeply understood from multiple perspectives. Given that dendrites will deform under the solute scouring in the solute convection theory and fragments may rotate freely in the mushy zone after fracture[37], it is believed that strain within these grains and misorientation of freckle grains relative to the matrix have a specific distribution. Therefore, in this work, scanning electron microscopy (SEM), energy dispersive x-ray spectroscopy (EDS), electron backscattering diffraction (EBSD), and aberration-corrected electron microscopy are used to analyze the misorientation angle (MA) and strain distribution in alloys with directionally solidified (247LC-DS and GTD111-DS) and single-crystal (René N4 and CMSX-4) structures. In addition, knowing that the intergrowth of borides in alloys usually follows a specific orientation relationship to the matrix[38-40], borides at the grain boundaries between freckles and matrix can also be used as a reference to further describe the movement regularity of freckle grains and their formation mechanism. Hereafter, unless otherwise specified, the samples are referred to as directionally solidified 247LC-DS alloys.

EXPERIMENTAL METHODS

Preparation of the blades

Four Nickel-based superalloys in this work are 247LC-DS, GTD111-DS, René N4, and CMSX-4, among which 247LC-DS and GTD111-DS are directionally solidified alloys, while René N4 and CMSX-4 are single crystal alloys (see the nominal chemical compositions in Table 1). Blades were prepared via Bridgman directional solidification technology, in which single crystal blades were obtained according to a spiral crystal selection method at the drawing speed of 4 mm/min. After solidification, shelling and sandblasting were carried out.

Sample preparation and data acquisition

The surface of blades was etched with a 50 vol.% HCL + 50 vol.% H_2O_2 solution to show the freckles. The freckle chains in the blade tenons and their surrounding matrix were cut into blocks with the sizes of 10 × 10 × 3 mm^3 using an electric spark cutter. Samples were stepwise polished with 240-5,000 grit silicon carbide sandpapers and then with 1 μm diamond grinding paste until their surfaces were scratch-free. After that, they were etched in 20 g of $CuSO_4$ + 100 mL HCL + 80 mL H_2O solution for 20 s prior to the optical microstructure observation on a Nikon ECLISE E200 setup.

The EBSD samples were prepared via mechanical polishing followed by electropolishing. The mechanical polishing procedure was the same as that described above. Electropolishing was conducted at 25 V and -25 °C for 20 s in a 10% vol $HCLO_4$ + 90% vol C_2H_5OH electrolyte. The EBSD tests were carried out on a Carl Zeiss Crossbeam 550 L instrument equipped with an Oxford Symmetry S2 EBSD console at a beam current of 25 nA at a voltage of 20 kV and a step size of 1.5 μm. The post-processing analysis of EBSD data was carried out using AZtec Crystal software. To analyze/quantify the internal stress along the freckles, the HR-EBSD measurements were performed using a mega-pixel pattern size of 1,024 × 1,344 at a speed of 20 Hz. The internal stress was then calculated using a Digital Image Correlation (DIC) method applied to the patterns. More detailed algorithms can be found in the previous article[41,42]. An Ultim Max EDS system as part of the Oxford Instrument was used to investigate the compositional distribution/element segregation at the dendrites and inter-dendrites at 20 kV and 2 nA.

Lamellae for transmission Kikuchi diffraction (TKD) and transmission electron microscopy (TEM) analyses were prepared through a focus ion beam (FIB) technique using Carl Zeiss Crossbeam 550 L equipment. The TKD patterns were collected at a beam current of 30 nA and a voltage of 30 kV. The Bright field (BF)

Table 1. Nominal composition of four kinds of alloys, in wt.% (Ni Bal.)

Alloy	Cr	Co	Al	Ti	Re	W	Mo	Ta	C	B	Nb	Hf	Zr
247LC-DS	8.0	9.0	5.6	0.8	-	9.5	0.5	3.2	0.07	0.015	-	1.4	0.015
GTD111-DS	14	9.5	3.0	4.9	-	3.8	1.5	2.8	0.1	0.01	-	< 0.15	-
René N4	9.5	7.5	4.2	3.5	< 0.1	6.0	1.5	4.8	0.06	0.04	0.5	0.15	< 0.01
CMSX-4	6.5	9.6	5.6	1	3	6.4	0.6	6.5	-	-	-	0.1	-

images, aberration-corrected high angle annular dark field (HAADF) images, and electron energy loss spectra (EELSs) were obtained by means of a Titan Themis Z setup equipped with a double aberration corrector at the operating voltage of 300 kV. Once the Z-contrast images at the atomic scale were taken, the convergence angle of the electron beam was set to 25 mrad.

RESULTS

Morphology and composition segregation of freckles

Figure 1A depicts a 247LC-DS blade, where the chain-like areas appearing in the white contrast along the solidification direction (the vertical direction in the figure) are freckle chains (indicated with black arrows). Figures 1B and Supplementary Figure 1 display the morphological SEM image and optical microscopy pattern of dendrites, respectively. The dendrites in the matrix are neatly arranged at the two sides, while the middle area resembles a channel containing carbides (B-containing alloy contains borides), shrinkage cavities, and randomly distributed grains, i.e., freckles.

Figure 1C depicts the crystal orientation distribution from the Y0 (IPFY) direction parallel to the solidification direction. Different colors in this figure indicate various crystallographic orientations, meaning that a freckle is composed of randomly oriented grains in contrast to a single-crystallized matrix. The same conclusion can be obtained from Figure 1D and the pole figure (PF) shown in Figure 1C, and the other three alloys also exhibit similar results. The MAs relative to the matrix of all freckle grains in four kinds of alloys were counted (the corresponding numbers of freckle grains for 247LC-DS, GTD111-DS, René N4, and CMSX-4 are 40, 31, 32, and 34, respectively), and the statistical data are given in Figure 1E. Two-thirds of freckle grains form an angle with the matrix in the range of 30-60 deg (the individual statistical results on four brands of alloys can be found in Supplementary Figure 2 of Supplementary Materials). According to the statistics on the freckle grain size with the equivalent circle diameter as a reference[43] [Figure 1F], the size of freckle grains is mostly within the range of 30-200 μm (the individual statistical results on four brands of alloys are shown in Supplementary Figure 3).

As we all know, Nickel-based superalloys usually contain more than ten kinds of elements that are randomly distributed in the alloy (see the element maps in Figure 2A). This has a significant impact on the properties of the alloy, such as the famous Re effect[44,45] (similar results were obtained for the other three alloys, as shown in Supplementary Figure 4). The segregation degree of an element in the alloy between dendrite and inter-dendrite can be expressed through the

element segregation coefficient K_i as follows:

$$K_i = C^i_{dendrite}/C^i_{inter\text{-}dendrite} \quad (1)$$

where $C^i_{dendrite}$ and $C^i_{inter\text{-}dendrite}$ are the mass fractions of the element between dendrite and inter-dendrite, respectively. If $K_i > 1$, the elements segregate in dendrites; at $K_i < 1$, the elements segregate in inter-dendrites. The EDS data were afterward collected at dendrites and inter-dendrites in the matrix and freckle areas, respectively, and the segregation coefficient of each element in the matrix and freckles for four alloys was calculated, as shown in Figure 2B-E. The segregation coefficients of W and Re (only CMSX-4 contains Re) are much greater than 1, indicating that these heavy elements with high melting points enrich the dendrites, while the light elements with low melting points, such as Al and Ti, are concentrated at the inter-dendrites. For dendrites during the solidification process, the addition of W and Re aggravates the density inversion, thus enhancing the solute convection and fostering the freckle formation, which is consistent with the experimental results[17]. Since the in-depth research on the composition has been reported in previous works[16,21-24], this paper mainly focuses on the orientation and strain.

Relationship between crystal orientation and strain

Hurricanes can cause the branches to bend or even fracture, and the sway and fracture of dendrites due to solute convection were similarly observed via ultrasound[46]. From this point of view, there should be different states during the whole convection process as to strain or orientation. For example, strain accumulating during deformation is relieved to some extent after fracture/breakage. Therefore, the microstructure of freckles in the four brands of alloys was further considered, and the correlation between the orientation and strain of freckle grains was analyzed to understand the formation mechanism of freckles.

Band contrast (BC) maps not only reflect the quality of the Kikuchi pattern during the EBSD data acquisition but also contain the channel contrast, which can be used to indicate the grain orientation to some extent. Hence, considering the BC map [Figure 3A] and the orientation map [Figure 3B], the area in the middle is referred to as freckles. It can be found from Figure 3B that the freckle grains with smaller MAs relative to the matrix mainly distribute near the interface between the freckle chain and matrix, while those with the larger MAs are mostly inside the freckle chain, which is in agreement with the statistics shown in Figure 3C (the individual statistical results on four brands of alloys are available in Supplementary Figure 5). Here, the MA of 2-10° is attributed to the low-angle grain boundary (LAGB), which is marked in Figure 3B with white curves and black arrows. Moreover, it is worth noting that in the BSE image [Figure 3D] corresponding to the area denoted with a black square in Figure 3B, five grains at the edge of freckle chains (outlined with a yellow dashed line) still maintain the secondary dendrite morphology and are arranged on the primary dendrite. However, their small MA means that they should be treated as freckle grains. Freckles in GTD111-DS, René N4, and CMSX-4 alloys were characterized, and similar results were obtained, as shown in Supplementary Figure 6. Therefore, it can be concluded that in this phenomenon, freckle grains with smaller MAs distribute near the interface, and those with larger MAs are present inside the freckle chain.

Kernel average misorientation (KAM) is usually used to qualitatively characterize the local strain as it represents the average value of the misorientation between the pixel at the center of the kernel and every other pixel within the kernel, which is essentially the result of deformation[47]. Therefore, the KAM is applied in this study to analyze the strain within all 117 freckle grains in four alloys. To avoid statistical errors due to the limited sample number, the results are displayed every ten degrees, as shown in Figure 4A. The abscissa

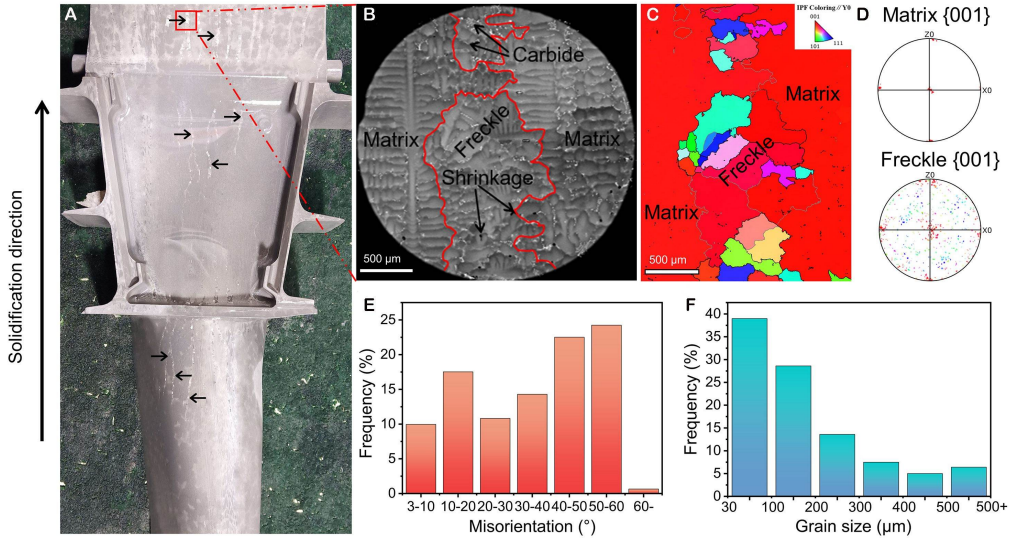

Figure 1. Dendrite morphology and grain orientation distribution within a freckle chain (the direction of solidification is from the bottom to the top). (A) Photograph of the turbine blade casting illustrating the presence of freckle chains (marked with black arrows). (B and C) BSE and orientation images of the freckle chain and the matrix corresponding to the area outlined with a red square in image (A). The interface is outlined with red curves, and carbides and shrinkage cavities are marked with black arrows. The orientation color legend is shown as the top-right inset. (D) Pole figures of the matrix and freckle, respectively, corresponding to the area highlighted in image (B). (E and F) Misorientation of freckle grains relative to the matrix and freckle grain size in four types of samples.

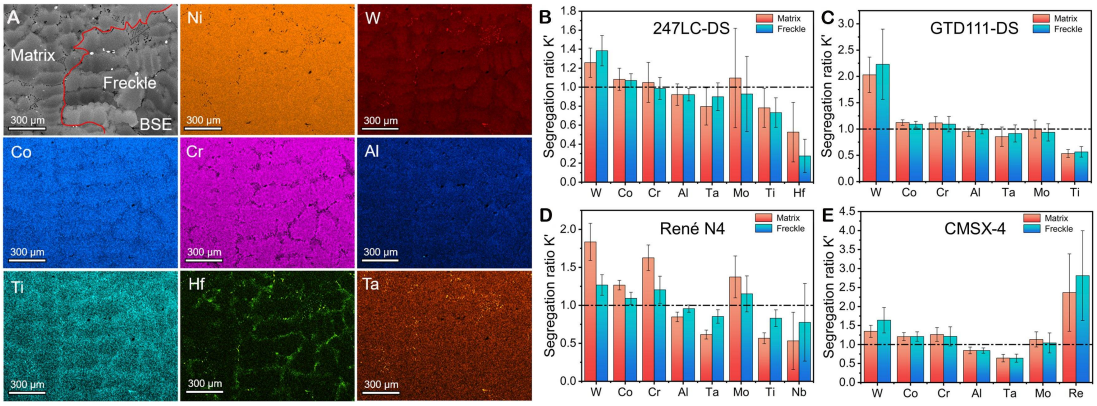

Figure 2. Element segregation analysis. (A) BSE image and EDS maps revealing the Ni, W, Co, Cr, Al, Ti, Hf, and Ta element distributions across the interface between the matrix and freckles. (B-E) Segregation coefficients of the matrix and freckle in 247LC-DS, GTD111-DS, René N4, and CMSX-4 alloys, respectively.

represents the MA of freckle grains relative to the matrix, and the ordinate is the average KAM value of grains (the individual statistical results on four brands of alloys are available in Supplementary Figure 7). It is found that the KAM value, i.e., strain, reaches the maximum value in the range of 20-30° and then decreases with a further increase of the MA.

It is well known that once the external force is removed from an object, the shape and volume changed by elastic strain will be restored. However, the plastic strain will persist in the form of crystal defects such as dislocations. Under the thermal-solute convection, the secondary dendrites are subjected to bending stress, which leads to the accumulation of plastic deformation. Meanwhile, the dendrites fractured and even entering the mushy zone are no longer subjected to bending stress but only the thermal-solute recovery,

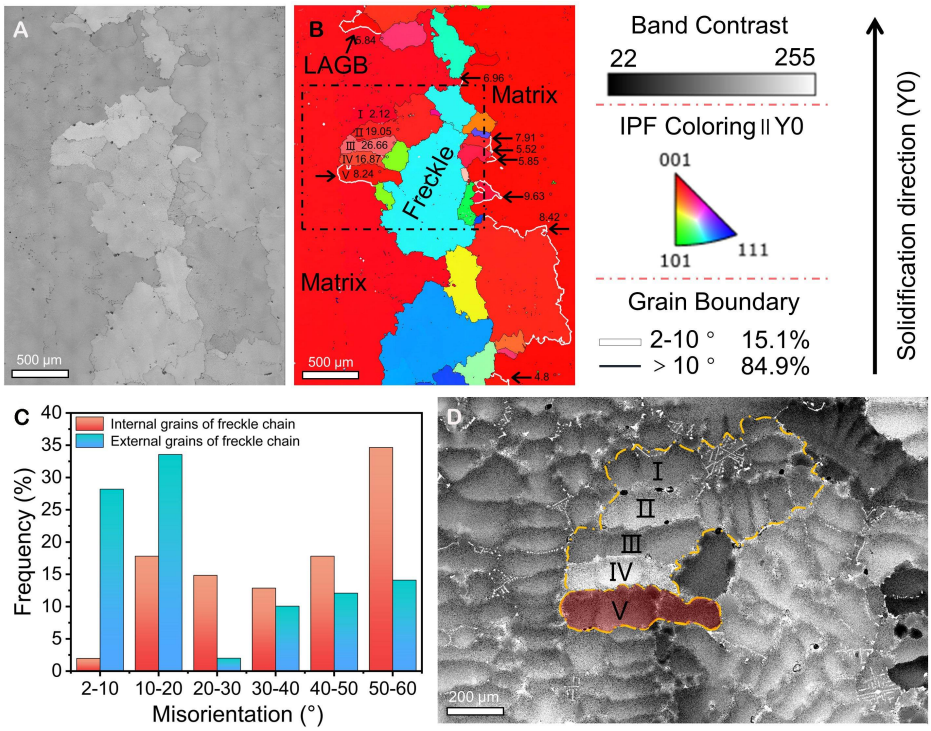

Figure 3. MA distribution in freckle grains. (A and B) Band contrast map and orientation map. LAGBs are highlighted with white lines, and their MAs are marked. (C) MA distributions for the internal and external grains. (D) BSE image corresponding to the black square in image (B), and five freckle grains are outlined with a yellow dashed line. The freckle grain marked in red is chosen for the HR-EBSD analysis.

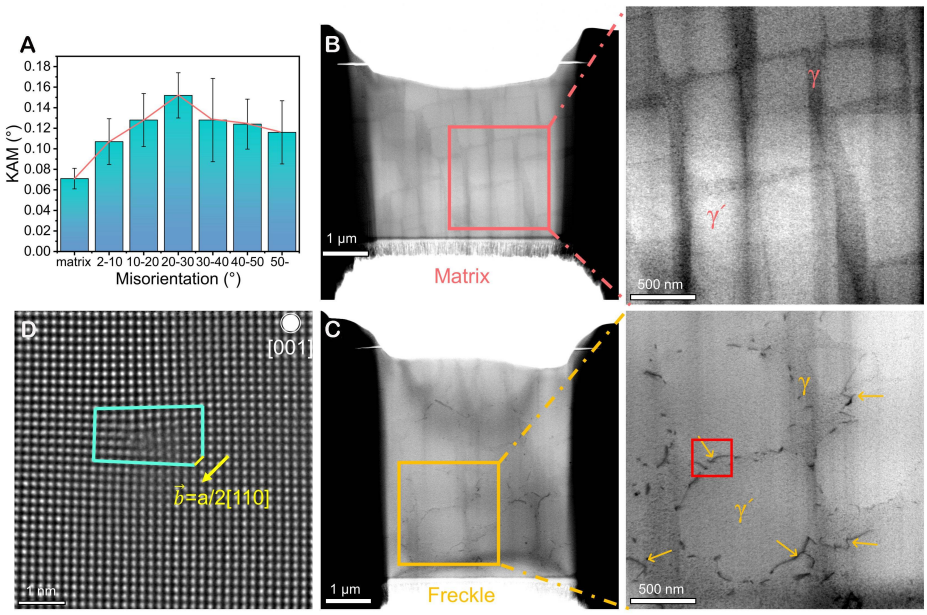

Figure 4. Plastic deformation of matrix and freckle grains. (A) Statistics on the KAM variation with MA in four brands of alloys. The orange curve is used to describe the trend. (B) BF-STEM images of the matrix. (C) BF-STEM images of the freckle grain. Dislocations are marked with yellow arrows. (D) High magnification HAADF-STEM image of the dislocation core, corresponding to the red square in image (C). Burgers vectors are determined by the Burgers circuit.

which leads to the partial recovery of plastic deformation[48,49]. Therefore, it is assumed from Figure 4A that the plastic deformation accumulated during the freckle formation is partially retained in the freckle grains; that is why the grains with MA above 50° KAM value are still larger than the matrix. If it is true, there should be more defects, such as dislocations or stacking faults, in freckles than in the matrix.

To prove the above speculation, the TEM sample was afterward made from the matrix and freckles, respectively. As shown in Figure 4B-D, the matrix and freckles are all composed of γ and γ′ phases, but there are no obvious dislocations in the matrix [Figure 4B], while lots of dislocations are found to grow along the γ/γ′ interface in freckles (marked with yellow arrows in Figure 4C), and one dislocation core is detected in Figure 4D. According to Figure 4, it can be inferred that in the process of freckle formation, the secondary dendrite undergoes plastic deformation as a result of solute convection, giving rise to a number of dislocations, which gradually build up enough crystallographic rotations. After the strain accumulates to a certain extent, grains fracture and enter the mushy zone to rotate freely so that the plastic strain is partially retained in freckles. One more thing that should be noted is that in the above-mentioned discussion, freckle grains with large MAs are predominately formed earlier than those with small MAs, as shown in Figures 3 and 4. Therefore, the earlier emerging grains lay in the center of the freckle, whereas those formed later are situated along the interface.

In order to further study the stress within dendrites caused by solute convection, the high-resolution (HR) EBSD (with a higher angular resolution than the traditional EBSD) KAM patterns were acquired to analyze the stress distribution inside the freckle grain. The red-highlighted grain with the MA of 8.24° in Figure 3D was characterized via the HR-EBSD, and the corresponding quantitative stress distribution is depicted in Figure 5. It can be seen that the stress directions on both sides of the grain are always opposite, and the e_{yy} stress component value (corresponding to the direction of solute convection during the directional solidification) is much larger than e_{xx} and e_{zz}. Meanwhile, the shear stress distributions exhibit the same trend, as shown in Supplementary Figure 8. This can be explained by the fact that the root of the secondary dendrite is connected with the matrix, and the other side of the dendrite is under the solute convection, which makes the two sides of the secondary dendrite undergo the opposite stress. Therefore, the strain distributions within freckles, displayed in Figure 5, seem reasonable in the context of the theory of solute convection. It needs to be specifically stated that the influence of solidification shrinkage and thermal stress cannot be ruled out, but solute convection is still the main factor in the strain distribution.

Before the secondary dendrites fracture, strain gradually increases at the grain boundary (GB) nearby through the deformation. In order to study the microstructure at the GB, the EBSD and FIB techniques were combined to accurately localize the interface. The TEM samples with a specific orientation were cut off, and their characterization was performed using the aberration-corrected electron microscope. As shown in the orientation map [Supplementary Figure 9A], the FIB treatment of the TEM sample was conducted at the position denoted with an arrow. Supplementary Figure 9B depicts the BF-STEM image of the interface, in which the left-hand side is the matrix, the right-hand side reveals freckles, and the MA of the LAGB in the middle is 4.64°. The atomic-resolution HAADF image of the interface (see Supplementary Figure 9C) shows that the two sides of the GB are basically coherent when the matrix is oriented along the [110] direction. To demonstrate the strain distribution at the interface, the geometric phase analysis (GPA) was carried out, as shown in Supplementary Figure 9D, and the chain of a strain-concentrated area under a synergistic effect of compressive and tensile strain can be observed along the GB. It is a dislocation core, as is evident from the high-magnification HAADF image [Supplementary Figure 9E], and its Burgers vector determined by the Burgers circuit is $\vec{b} = a/2[110]$, which is common for this alloy. Therefore, the strain within the LAGB originates from a series of edge dislocations.

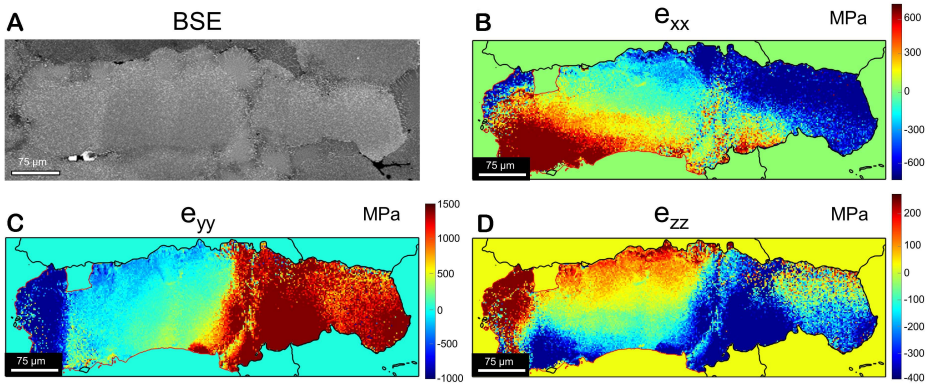

Figure 5. Normal stress distribution obtained by the HR-EBSD measurements. (A) BSE image of the freckle grain marked in red in Figure 3D. (B-D) Distributions of stress components e_{xx}, e_{yy}, and e_{zz}, respectively.

Deflection behavior of borides at the interface

As a GB strengthening element, boron is often added to nickel-based superalloys to improve their creep properties[50,51]. Usually, borides are settled at the grain boundaries[52], and there is a specific orientation relationship between borides and alloys[38-40]. Therefore, the orientation relationship between borides and alloys can be used to indirectly study the deflection behavior of freckle grains. In this work, a TEM sample was prepared at the GB between the red-highlighted freckle grain and the left-hand matrix in Figure 3D, and the orientation and interfacial structure were characterized via TKD and aberration-corrected electron microscopy, as shown in Figure 6. In the BF image [Figure 6A], a LAGB is marked with a red dashed line, with the matrix on the left and the freckle on the right. Combined with a TKD - phase distribution map [Figure 6B], it can be seen that M_5B_3 borides exist at the γ/γ′ phase boundary (PB) and the GB. The EDS results [Supplementary Figure 10A] reveal that the heavy elements present in borides are Cr and W. However, since EDS is insensitive to B elements with a small atomic number, the EELS [Supplementary Figure 10B] experiments were carried out to obtain the signal from boron. By combining the EDS and EELS results, the composition of borides is confirmed to be close to M_5B_3, as shown in Supplementary Figure 10C, which is consistent with the calibration data on TKD. In order to establish the orientation relationship between borides and matrix or freckles more intuitively, three-dimensional unit cells of the matrix, freckle, and Boride were overlaid on the IPF map, as shown in Figure 6C.

Four borides in Figure 6A were selected for further analysis. Among them, boride 1 is located at the γ/γ′ interface in the matrix, and the HAADF image of the interface is depicted in Figure 6D, whereas the high-magnification HAADF image of the [130]-oriented M_5B_3 is shown as the top-right inset. Because the contrast of the HAADF image is proportional to the atomic number $Z^{1.7}$, it is impossible to display the B atom via HAADF. Therefore, the bright dots in the image represent M (namely Cr and W) atoms, and the experimental image matches the model very well. Combined with the fast Fourier transformation (FFT) scan of the corresponding area [Figure 6E], it can be seen that there is a $[001]_M//[130]_B$ orientation relationship between borides and matrix, which is consistent with the literature[40]. According to the HAADF image of the interface [Figure 6F], the matrix smoothly transits into the M_5B_3 phase and the interface is completely coherent, which is in agreement with Figure 6E.

Unlike boride 1, borides 2-4 are located at the LAGB between the matrix and freckles, and the deflection occurs in different degrees. The orientation relationship between boride 2 and the matrix is similar to that for boride 1; that is, borides are almost coherent with the matrix, which is confirmed by Figure 6G-I. An almost identical trend is obtained for boride 4, but with respect to the freckle grain and not with the matrix

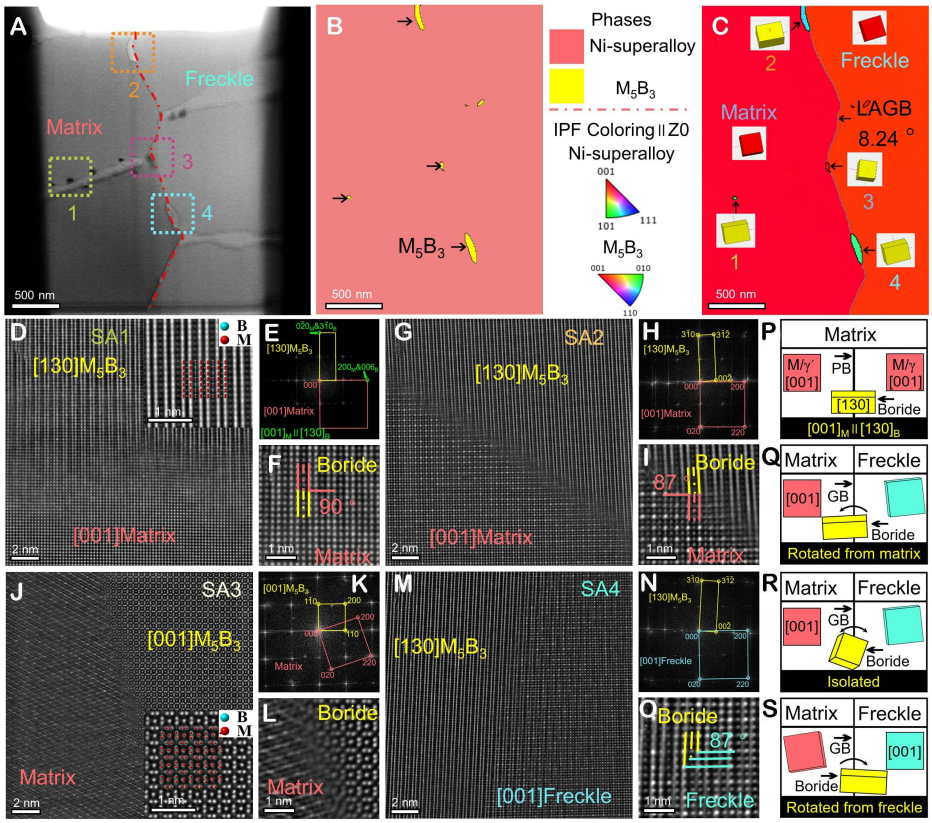

Figure 6. Deflection behavior of borides. (A) BF-STEM image of M_5B_3 borides sampled from the interface between the matrix and the freckle. Among them, four borides were selected for further study, in which boride 1 is located at the γ/ phase boundary and the others are at the grain boundary. (B) A TKD - phase distribution map, in which borides are marked with black arrows. (C) A TKD - orientation map, in which three-dimensional unit cells of matrix, freckles, and borides are shown to understand their orientation relationship. (D-O) HAADF-STEM, FFT, and high-magnification HAADF-STEM images of the interface between alloys and borides 1-4. (P-S) Schematic diagrams of four borides, respectively.

[Figures 6M-O]. Borides 2 and 4 are deflected by 3° in different directions on the basis of the original specific orientation. In turn, for boride 3, there is a large misorientation, as shown in Figure 6J-L.

According to Figure 6, borides have a specific orientation relationship with the matrix, such as boride 1, and the corresponding schematic diagram is shown in Figure 6P. However, when borides are located at the interface between the matrix and freckles, there is the MA between borides and the matrix or freckles, which may be due to the solute scouring. Three situations may exist for borides: they can be almost attached to the matrix (boride 2 in Figure 6Q) or to the freckle (boride 4 in Figure 6S), or alternatively, they may exist independently from the matrix and freckles (boride 3 in Figure 6R). In a word, it is assumed that solute scouring weakens the original orientation relationship between borides and alloys in different degrees. Thus, the deflection behavior of borides relative to alloys can be understood based on the solute scouring on the dendrite in the context of the solute convection theory.

DISCUSSION

As shown in Figure 7A, in the process of directional solidification, the alloy grows from the bottom to the top in the form of dendrites, with the primary dendrite orientation along the <001> direction, which is basically consistent with the heat flow direction. Generally, the alloy is divided into three areas from bottom to top: a solid area, a mushy zone (a mixture of solid and liquid), and a liquid area. In the horizontal

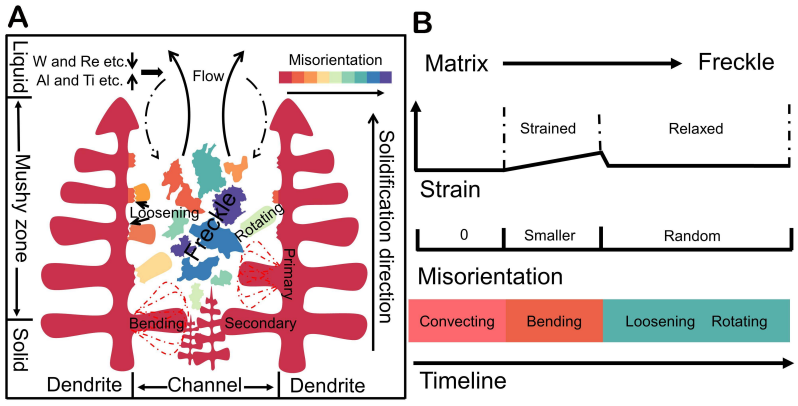

Figure 7. Freckle formation mechanism. (A) schematic diagram of freckle formation and chain formation process; (B) the relationship between orientation and strain in different stages of freckle formation.

direction, it is divided into two parts: a freckle channel in the middle and primary dendrites on the two sides.

During the directional solidification, the dendrite solidifies first at the bottom, meaning that heavy elements, such as W and Re, segregate. As a result, the density of the liquid at the bottom of the dendrite is lower than that near the tip of the dendrite on the top. Then, the density inversion makes the liquid with low density in the mushy zone flow upward, leading to the solute convection.

Thanks to the solute convection, the secondary dendrites on both sides of the channel will be scoured to sway, loosen, or even fracture. Thus, according to different conditions of dendrites, the freckle formation can be divided into two stages, namely strained and relaxed stages, as shown in Figure 7B. The local strain in the grains gradually rises, increasing the deformation before fracture, which corresponds to the left-hand side of the KAM peak (the 20-30° range in Figure 4A), meaning the strained state. Meanwhile, the relaxed state indicates that secondary dendrites are fractured and even enter the mushy zone, causing the local strain in the grain to decrease (the plastic strain is partially retained), which corresponds to the right-hand side of the KAM peak. From the viewpoint of the MA, freckle grains are bent in a strained state due to the continuous scouring of the solute; as a result, the MA increases with more deformation. Once a limit is achieved, secondary dendrites will loosen, reaching the relaxed state and increasing the MA relative to that in the strained state. When grains sink into the mushy zone, the latter starts to roll unrestrained, leading to the random orientation of freckles. As soon as this area is solidified, freckle grains take shape, and with the growth of alloys along the <001> direction, more grains come to the channel, allowing for the formation of freckle chains at the end of solidification. Therefore, based on the composition, strain, and orientation data analysis [Figures 2-7], it can be confirmed that the formation of freckles coincides with the theory of solute convection, including solute segregation, density inversion, and dendrite fracture.

However, in the whole solidification process, the two most important influencing factors are the temperature field and solute field, while solidification technology, alloy compositions, and casting structures and sizes will lead to the variation of these two factors, making the real solidification process more complex[9]. In addition, the effect of solidification shrinkage and thermal stress on freckle formation is also unavoidable. Given the limitation of technical means, only the microstructure after the formation of freckles is considered in this study, and a lot of experimental and numerical simulation work still needs to be done.

CONCLUSION

Using SEM, EBSD, and aberration-corrected electron microscopy tools, the composition, orientation, and strain of freckle grains in four Nickel-based alloys and borides from the mesoscopic scale to the microscopic scale were investigated. Based on the experimental results, the main conclusions can be drawn as follows.

(1) Freckle grains with smaller MAs are distributed near the interface between the freckles and matrix, and those with larger MAs are inside the freckle chains.

(2) Strain of the freckle grain gradually increases with the MA, meaning the increase of deformation before fracture, which corresponds to the left-hand side of the KAM peak (20-30°), named the strained state. In the relaxed state corresponding to the right-hand side of the KAM peak, the local strain is relaxed, indicating that secondary dendrites are fractured with the partial retention of plastic strain.

(3) The stress directions on both sides of the secondary dendrite are always opposite, and the stress along the direction of solute scouring is much higher.

(4) Borides in the matrix usually intergrow with the alloy, conforming to the specific orientation relationship. There is some deviation when borides are located at the boundary between the matrix and freckles.

The experimental results of this work ensure additional proof for the theory of thermal-solutal convection and enrich the methodology of freckle studies, providing new insight into the formation mechanism of casting defects.

DECLARATIONS

Author contribution

Supervised the project: Ge B
Conceived the experiments: Wang S, Jia Y, Zhang Y, Shen X, Cheng F, Ge B
Prepared turbine blades: Jia Y, Du Y
Analyzed the EBSD data: Wang S, Ma L
Performed the HREBSD experiments and analyzed the HREBSD data: Wang Y, Zeng Y
Prepared the manuscript: Wang S, Jia Y, Wang Y, Zeng Y, Ma L, Zeng Y, Shen X, Ge B
All authors discussed the results and contributed to the manuscript.

Availability of data and materials

The data that support the findings of this study are available from the corresponding author upon reasonable request.Supplemental Information can be found online.

Financial support and sponsorship

This work has been supported by the Anhui Science and Technology Major Project (acceptance number: S2019b05050019), the National Natural Science Foundation of China (No. 11874394), and the University Synergy Innovation Program of Anhui Province (No. GXXT-2020-003).

Conflicts of interest

All authors declared that there are no conflicts of interest.

Ethical approval and consent to participate

Not applicable.

Consent for publication

Not applicable.

Copyright

© The Author(s) 2024.

REFERENCES

1. Broomfield RW, Ford DA, Bhangu JK, et al. Development and turbine engine performance of three advanced rhenium containing superalloys for single crystal and directionally solidified blades and vanes. Proceedings of the ASME 1997 International Gas Turbine and Aeroengine Congress and Exhibition. 1997 Jun 2-5; Orlando, USA. New York: ASME; 1998. DOI
2. Gasson PC. *The superalloys: fundamentals and applications*. R. C. Reed Cambridge University Press, The Edinburgh Building, Shaftesbury Road, Cambridge, CB2 2RU, UK, 2006. 372pp. Illustrated. £80. ISBN 0-521-85904-2. *Aeronaut j* 2008;112:291. DOI
3. Pollock T, Argon A. Creep resistance of CMSX-3 nickel base superalloy single crystals. *Acta Metall Mater* 1992;40:1-30. DOI
4. Versnyder FI, Shank M. The development of columnar grain and single crystal high temperature materials through directional solidification. *Mater Sci Eng* 1970;6:213-47. DOI
5. Quested PN, Osgerby S. Mechanical properties of conventionally cast, directionally solidified, and single-crystal superalloys. *Mater Sci Technol* 1986;2:461-75. DOI
6. Giamei AF, Kear BH. On the nature of freckles in nickel base superalloys. *Metall Trans* 1970;1:2185-92. DOI
7. Chmiela B, Sozańska M, Cwajna J. Identification and evaluation of freckles in directionally solidified casting made of PWA 1426 nickel-based superalloy. *Arch Metall Mater* 2012;57:559-64. DOI
8. Worster MG. Instabilities of the liquid and mushy regions during solidification of alloys. *J Fluid Mech* 1992;237:649-69. DOI
9. Ramirez JC, Beckermann C. Evaluation of a rayleigh-number-based freckle criterion for Pb-Sn alloys and Ni-base superalloys. *Metall Mater Trans A* 2003;34:1525-36. DOI
10. Valdés J, King P, Liu X. On the formulation of a freckling criterion for Ni-based superalloy vacuum arc remelting ingots. *Metall Mater Trans A* 2010;41:2408-16. DOI
11. Frueh C, Poirier D, Felicelli S. Predicting freckle-defects in directionally solidified Pb-Sn alloys. *Mater Sci Eng* 2002;328:245-55. DOI
12. Wang F, Ma D, Zhang J, Bogner S, Bührig-polaczek A. Solidification behavior of a Ni-based single crystal CMSX-4 superalloy solidified by downward directional solidification process. *Mater Charact* 2015;101:20-5. DOI
13. Li Q, Shen J, Qin L, Xiong Y, Yue X. Effect of traveling magnetic field on freckle formation in directionally solidified CMSX-4 superalloy. *J Mater Process Technol* 2019;274:116308. DOI
14. Li Q, Shen J, Qin L, Xiong Y. Investigation on local cooling in reducing freckles for directionally solidified superalloy specimens with abruptly varying cross-sections. *Mater Charact* 2017;130:139-48. DOI
15. Xiao J, Jiang W, Han D, Li K, Lu Y, Lou L. Evolution of crystallographic orientation and microstructure in the triangular adapter of grain continuator of a 3rd-generation single crystal superalloy casting during directional solidification. *J Alloys Compd* 2022;898:162782. DOI
16. Genereux PD, Borg CA. Characterization of freckles in a high strength wrought nickel superalloy. *Superalloys* 2000;2000:19-27. Available from: https://www.tms.org/superalloys/10.7449/2000/Superalloys_2000_19_27.pdf [Last accessed on 20 Dec 2023].
17. Pollock TM, Murphy WH, Goldman EH, Uram DL, Tu JS. Grain defect formation during directional solidification of nickel base single crystals. *Superalloys* 1992;1992:125-34. Available from: https://www.tms.org/superalloys/10.7449/1992/Superalloys_1992_125_134.pdf [Last accessed on 20 Dec 2023].
18. Sarazin JR, Hellawell A. Channel formation in Pb-Sn, Pb-Sb, and Pb-Sn-Sb alloy ingots and comparison with the system NH_4Cl-H_2O. *Metall Trans A* 1988;19:1861-71. DOI
19. Karagadde S, Yuan L, Shevchenko N, Eckert S, Lee P. 3-D microstructural model of freckle formation validated using in situ experiments. *Acta Mater* 2014;79:168-80. DOI
20. Ren N, Li J, Panwisawas C, Xia M, Dong H, Li J. Thermal-solutal-fluid flow of channel segregation during directional solidification of single-crystal nickel-based superalloys. *Acta Mater* 2021;206:116620. DOI
21. Amouyal Y, Seidman D. An atom-probe tomographic study of freckle formation in a nickel-based superalloy. *Acta Mater* 2011;59:6729-42. DOI
22. Tin S, Pollock TM, King WT. Carbon additions and grain defect formation in high refractory nickel-base single crystal superalloys. *Superalloys* 2000;2000:201-10. Available from: https://www.tms.org/Superalloys/10.7449/2000/Superalloys_2000_201_210.pdf [Last accessed on 20 Dec 2023].
23. Tin S, Pollock TM, Murphy W. Stabilization of thermosolutal convective instabilities in Ni-based single-crystal superalloys: carbon additions and freckle formation. *Metall Mater Trans A* 2001;32:1743-53. DOI

24. Amouyal Y, Seidman D. The role of hafnium in the formation of misoriented defects in Ni-based superalloys: an atom-probe tomographic study. *Acta Mater* 2011;59:3321-33. DOI
25. Karagadde S, Lee PD, Cai B, et al. Transgranular liquation cracking of grains in the semi-solid state. *Nat Commun* 2015;6:8300. DOI PubMed PMC
26. Cai B, Wang J, Kao A, et al. 4D synchrotron X-ray tomographic quantification of the transition from cellular to dendrite growth during directional solidification. *Acta Mater* 2016;117:160-9. DOI
27. Reinhart G, Grange D, Abou-khalil L, et al. Impact of solute flow during directional solidification of a Ni-based alloy: in-situ and real-time X-radiography. *Acta Mater* 2020;194:68-79. DOI
28. Ren N, Panwisawas C, Li J, Xia M, Dong H, Li J. Solute enrichment induced dendritic fragmentation in directional solidification of nickel-based superalloys. *Acta Mater* 2021;215:117043. DOI
29. Isensee T, Tourret D. Convective effects on columnar dendritic solidification - a multiscale dendritic needle network study. *Acta Mater* 2022;234:118035. DOI
30. Mullis A. Growth induced dendritic bending and rosette formation during solidification in a shearing flow. *Acta Mater* 1999;47:1783-9. DOI
31. Dragnevski K, Mullis AM, Walker DJ, Cochrane RF. Mechanical deformation of dendrites by fluid flow during the solidification of undercooled melts. *Acta Mater* 2002;50:3743-55. DOI
32. Billia B, Bergeon N, Thi HN, Jamgotchian H, Gastaldi J, Grange G. Cumulative mechanical moments and microstructure deformation induced by growth shape in columnar solidification. *Phys Rev Lett* 2004;93:126105. DOI PubMed
33. Niederberger C, Michler J, Jacot A. Origin of intragranular crystallographic misorientations in hot-dip Al-Zn-Si coatings. *Acta Mater* 2008;56:4002-11. DOI
34. Yuan L, Lee PD. A new mechanism for freckle initiation based on microstructural level simulation. *Acta Mater* 2012;60:4917-26. DOI
35. Ananiev S, Nikrityuk P, Eckert K. Dendrite fragmentation by catastrophic elastic remelting. *Acta Mater* 2009;57:657-65. DOI
36. Boden S, Eckert S, Willers B, Gerbeth G. X-ray radioscopic visualization of the solutal convection during solidification of a Ga-30 Wt Pct In Alloy. *Metall Mater Trans A* 2008;39:613-23. DOI
37. Appolaire B, Albert V, Combeau H, Lesoult G. Free growth of equiaxed crystals settling in undercooled NH_4Cl-H_2O melts. *Acta Mater* 1998;46:5851-62. DOI
38. Hu X, Zhu Y, Ma X. Crystallographic account of nano-scaled intergrowth of M_2B-type borides in nickel-based superalloys. *Acta Mater* 2014;68:70-81. DOI
39. Ge H, Liu J, Zheng S, et al. Boride-induced dislocation channeling in a single crystal Ni-based superalloy. *Mater Lett* 2019;235:232-5. DOI
40. Du B, Shi Z, Yang J, et al. M5B3 boride at the grain boundary of a nickel-based superalloy. *J Mater Sci Technol* 2016;32:265-70. DOI
41. Wang Y, Brodusch N, Gauvin R, Zeng Y. Line-rotated remapping for high-resolution electron backscatter diffraction. *Ultramicroscopy* 2022;242:113623. DOI PubMed
42. Wilkinson AJ, Meaden G, Dingley DJ. High-resolution elastic strain measurement from electron backscatter diffraction patterns: new levels of sensitivity. *Ultramicroscopy* 2006;106:307-13. DOI PubMed
43. Mingard K, Roebuck B, Bennett E, et al. Comparison of EBSD and conventional methods of grain size measurement of hardmetals. *Int J Refract Hard Met H* 2009;27:213-23. DOI
44. Mottura A, Reed RC. What is the role of rhenium in single crystal superalloys? *MATEC Web Conf* 2014;14:01001. DOI
45. Huang M, Zhu J. An overview of rhenium effect in single-crystal superalloys. *Rare Met* 2016;35:127-39. DOI
46. Wang S, Kang J, Guo Z, et al. In situ high speed imaging study and modelling of the fatigue fragmentation of dendritic structures in ultrasonic fields. *Acta Mater* 2019;165:388-97. DOI
47. Wright SI, Nowell MM, Field DP. A review of strain analysis using electron backscatter diffraction. *Microsc Microanal* 2011;17:316-29. DOI PubMed
48. Gottstein G. Physical foundations of materials science. Berlin:Springer;2004. DOI
49. Callister W. Materials science and engineering: an introduction (2nd edition). *Mater Des* 1991;12:59. DOI
50. Floreen S, Davidson JM. The effects of b and Zr on the creep and fatigue crack growth behavior of a Ni-base superalloy. *Metall Trans A* 1983;14:895-901. DOI
51. Li X, Ou M, Wang M, Zhang L, Ma Y, Liu K. Effect of boron addition on the microstructure and mechanical properties of K4750 nickel-based superalloy. *J Mater Sci Technol* 2021;60:177-85. DOI
52. Kontis P, Yusof HM, Pedrazzini S, et al. On the effect of boron on grain boundary character in a new polycrystalline superalloy. *Acta Mater* 2016;103:688-99. DOI